The 12 900 years BP Laacher See eruption: estimation of volatile yields and simulation of their fate in the plume

C. TEXTOR[1,*], P. M. SACHS[2,†], H.-F. GRAF[3] & T. H. HANSTEEN[2]

[1]Max-Planck Institute for Meteorology, Bundestraße 55, D-20146 Hamburg, Germany.
(e-mail: textor@dkrz.de)
[2]Forschungszentrum GEOMAR, Vulkanologie und Petrologie, Wischhofstraße 1–3, D-24148, Kiel, Germany.
[3]Max-Planck Institute for Meteorology, Bundestraße 55, D-20146 Hamburg, Germany.

Abstract: We estimated the volatile emissions of the 12 900 years BP eruption of Laacher See volcano (Germany), using a modified petrological method. Glass inclusions in phenocrysts and matrix glasses sampled over the Laacher See tephra profile were analysed by synchrotron X-ray fluorescence microprobe and electron microprobe to obtain the emitted masses of halogens, sulphur, and water. These data were used to initialize the numerical plume model ATHAM in order to investigate the fate of volcanic gases in the plume, and to estimate volatile masses injected into the stratosphere. The scavenging efficiency of each volatile component depends on its interactions with both liquid water and ice. We found a scavenging efficiency of *c.* 5% for the sulphur species, and of only *c.* 30% for hydrogen halides, despite their high water solubility. Our simulations showed that the greatest fraction of hydrometeors freeze to ice, due to the fast plume rise and great height of the eruption column. For the dry atmospheric conditions of the Laacher See eruption, the amount of liquid water was not sufficient to completely scavenge HCl and HBr, so that a large proportion could reach the stratosphere.

Volcanic eruptions reach the stratosphere, on average, at least once every two years (Simkin 1993). Plinian eruptions contribute to the stratospheric sulphate aerosol via injection of sulphur gases that are subsequently oxidized to form sulphate aerosol. Volcanic sulphur is emitted primarily as sulphur dioxide (SO_2) and hydrogen sulphide (H_2S). The H_2S is oxidized within days to SO_2 (e.g. McKeen 1984), which, in turn, is oxidized to sulphate, with a lifetime of approximately 35 days in the dry stratosphere (Bluth *et al.* 1992). The stratospheric aerosol burden can be significantly enhanced in the years following major volcanic eruptions. Sulphate aerosols in the stratosphere have radiative effects, altering the Earth's radiation balance (e.g. Charlson *et al.* 1991, 1992; Stenchikov *et al.* 1998), and hence can influence the global climate. A reduction of stratospheric ozone after large volcanic eruptions has also been observed. The column ozone reduction after the 1991 Mount Pinatubo eruption, which could be attributed to the volcanic effect, ranged from about 2% in the tropics, to about 7% at mid latitudes (Angell 1997; Solomon *et al.* 1998). The observed ozone changes are a combined effect of perturbations in heating and photolysis rates, and in stratospheric chemistry. Volcanic hydrated sulphate aerosols can serve as sites for heterogeneous reactions, which destroy ozone in the presence of halogens by converting passive halogen compounds into active ones (e.g. Hofmann & Solomon 1989; Granier & Brasseur 1992; Solomon *et al.* 1996). Hence, the increase in stratospheric halogens caused by anthropogenic activities has caused the observed decrease in stratospheric ozone after major volcanic eruptions. Since the human-induced increase of chlorine concentration in the stratosphere has peaked, the effect of ozone destruction by volcanic aerosol will probably decrease in the next few decades (Brasseur *et al.* 1990; Tie & Brasseur 1995).

*Author to whom correspondence should be addressed.
†Deceased.

From: OPPENHEIMER, C., PYLE, D.M. & BARCLAY, J. (eds) 2003 *Volcanic Degassing*. Geological Society, London, Special Publications, **213**, 307–328. 0305–8719/03/$15.00

The amount of volcanic sulphur injected into the stratosphere during a Plinian eruption is difficult to determine exactly with the methods available (e.g. Rose *et al.* 2000). The quantification of gas and particle concentrations in a volcanic plume is challenging, because of the cloud's opacity and the inherent risks of direct observation and sampling. Volcanic emissions can be studied remotely by airborne and ground-based instruments, and by satellite observations. The significant differences in the observational data are due to uncertainties in each individual measuring technique, but they also result from the fact that the plume is investigated at different distances from the crater and during different states of volcanic activity. Changes in the emissions at (and between) single sources over orders of magnitude can take place depending on levels of activity (and magma type).

A post-eruptive increase in the amount of stratospheric SO_2 on the second day after the eruption has been observed by the TOMS instrument (see Carn *et al.*, 2003, Chapter 11, this volume) after several explosive volcanic eruptions (Bluth *et al.*1995). The reason for this post-eruptive increase is not yet clear. The favoured explanation is that the additional SO_2 stems from the oxidation of co-emitted H_2S, which cannot be detected by the TOMS instrument (Rose *et al.* 2000). The magmatic H_2S fraction increases with increasing pressure (i.e. depth of the magma chamber) and with decreasing temperature and oxygen activity of the magma (Gerlach *et al.* 1986). Another reason could be the release of SO_2, which had been incorporated into frozen hydrometeors during the plume rise, when these hydrometeors sublimate in the dry stratosphere (Rose *et al.* 2001). Indications of ice in volcanic plumes were found in the eruption columns of Redoubt in 1989–1990 (Schneider *et al.* 1994), Rabaul in 1994 (Rose *et al.* 1995), Soufrière Hills Volcano, Montserrat in 1998–1999 (Mayberry *et al.* 2001), Hekla in February 2000 (Rose *et al.* 2000; Krotkov & Krueger 2000), and in the 1992 Mount Spurr eruption cloud (Rose *et al.* 2001). Unusually low concentrations of SO_2, together with high ice concentration, are suggestive of gas scavenging by ice (Rose *et al.* 1995, 2001). The stability of ice in the stratosphere, which could subsequently release SO_2, is dependent on the amount of water in the plume, which is in turn dependent on the volcanic and environmental conditions. An increased concentration of H_2O could accelerate SO_2 or H_2S oxidation in the stratosphere. In addition, it would influence the composition of sulphate aerosol, and hence the radiative effects of the eruption. The amount of H_2O (vapour and ice) injected into the stratosphere during a volcanic eruption has not yet been quantified, but can be substantial because of the tropospheric water entrained into the rising plume, which is generally considered to far exceed the amount of magmatic water. Numerical simulations with a 'top-hat' model indicated that large volcanic eruptions could deposit a mass of water in the stratosphere equivalent to up to 7% of the total stratospheric water burden (Glaze *et al.* 1997).

Direct injection of halogens into the stratosphere during a Plinian eruption could enhance ozone destruction. The volcanic emission of halogens can be significant (e.g. Varekamp *et al.* 1984; Westrich *et al.* 1992), but after the eruption of Mount Pinatubo the concentration of HCl in the stratosphere was not significantly enhanced (e.g. Mankin *et al.* 1992; Wallace & Livingston 1992). On the other hand, a clear increase in chlorine concentration was detected after the eruption of El Chichón in 1982, (Mankin & Coffey 1984; Woods *et al.* 1985). Until now, little attention has been paid to the potential stratospheric effects of heavy halogens released from volcanoes, such as bromine and iodine (Sachs & Harms 1998, 2000; Bureau *et al.* 2000). Bromine atoms are about 60 times more effective in destroying ozone than chlorine atoms (Daniel *et al.* 1995; Montzka *et al.* 1996).

The proportion of volcanic volatiles injected into the stratosphere by a Plinian eruption in relation to those erupted at the vent is governed by the scavenging efficiency of the individual species. Tabazadeh and Turco (1993) investigated the scavenging of HCl and SO_2 in an explosive volcanic plume using a one-dimensional, steady-state 'top-hat' model (Wilson 1976; Woods 1988; Woods 1993). The temperature distribution in the plume was obtained from this model. It was assumed that the existence of supercooled droplets was favoured as compared with ice formation. The authors argued that ice nucleation requires cooling below –20 ºC, as in typical meteorological convective clouds. The scavenging of chemical species in the eruption column was parameterized by assuming solubility equilibrium in these supercooled droplets. The concentration of volatiles remaining in the gas phase was derived from sophisticated thermodynamic theory.

Tabazadeh and Turco (1993) concluded that HCl was almost completely transferred into supercooled droplets, resulting in an HCl vapour pressure reduction of up to four orders of magnitude. On the other hand, it was found that the scavenging of SO_2 in the eruption column was insignificant: due to its low solubility in

liquid water it reaches the stratosphere almost unaffected by any scavenging in the plume. Although the study of Tabazadeh and Turco (1993) stands as an important first attempt to simulate the chemistry in a Plinian plume and considers a complex thermodynamic theory for phase equilibrium, it was based on a relatively simple treatment of the dynamics, and it did not consider cloud microphysical processes. In their simulations, all hydrometeors were liquid, and incorporation of gases in ice particles was not considered. The parameters that determine the scavenging efficiency need to be further investigated for different volcanic and environmental conditions.

In this chapter we describe the experimental set-up to estimate the amount of volatiles released by the 12 900 years BP Laacher See eruption. We then explain the processes occurring in the eruption column, which determine the scavenging efficiency of these volatiles during plume rise. In the last part, we present numerical simulations with the non-hydrostatic plume model ATHAM (**A**ctive **T**racer **H**igh Resolution **A**tmospheric **M**odel) for conditions similar to the Laacher See eruption, including scavenging processes in the eruption column. These simulations provide an estimate of the potential injection of sulphur and halogen gases into the stratosphere.

Laacher See volcano

Volcanological and petrological background

The magnitude of the 12 900 years BP Laacher See eruption has been estimated at between 5.1 and 6.3 km^3 DRE (dense rock equivalent) (Bogaard & Schmincke 1985; Schmincke *et al.* 1999; Harms & Schmincke 2000). In the following we will use an average value of 5.6 km^3. The proximal tephra sequence is subdivided into three major units: Lower Laacher See Tephra (LLST, first Plinian stage, dominantly fallout except for the most proximal facies), Middle Laacher See Tephra (MLST A, B, C; second Plinian stage, dominantly pyroclastic flows in the lower, and alternating fallout and flow in the upper part) and Upper Laacher See Tephra (ULST, phreatomagmatic stage with dominantly surge breccias, dunes and flows). The distribution of Laacher See tephra fallout is shown in Figure 1.

The Laacher See phonolite tephra sequence represents an inverted, chemically zoned magma reservoir. Miaskitic (Na+K/Al<1) and peralkaline phonolites (Na+K/Al>1), represent the lowermost mafic and the uppermost differentiated erupted portion of the Laacher See magma chamber, respectively. Fractionation calculations indicate that the erupted phonolitic magma could be derived from 56 km^3 of parental basanite magma (Wörner & Schmincke 1984*a*, *b*). The pressure was between 100 and 200 MPa (Wörner *et al.* 1985). The temperature in the upper part of the magma reservoir was <760 °C (probably down to 720 °C in the most differentiated levels). Temperatures >840–860 °C prevailed in the lower part, as indicated by experimental determination of the phase relationships (Harms 1998; Berndt *et al.* 2001).

The earliest erupted phonolites are almost aphyric, while those erupted near the end contain up to 40 vol.% crystals (mainly plagioclase, sanidine, clinopyroxene, amphibole, phlogopite, hauyne, titanite, magnetite, apatite, olivine). Amphibole/clinopyroxene phenocryst ratios show a roof-ward increase in the magma chamber (Tait *et al.* 1989). Crystal cumulates are common in the upper part of the tephra deposit; they range from syenites to clinopyroxenites and hornblendites (Tait 1988; Tait *et al.* 1989). Xenoliths comprise fragments of quartz–feldspar gneisses, mica schists, Devonian slates and greywacke.

Analytical methods

We estimated masses emitted of S, F, Cl, Br, I, and H_2O over the entire Laacher See tephra profile. Glass inclusions in phenocrysts and matrix glasses were analysed by synchrotron X-ray fluorescence microprobe (SYXRF) and electron microprobe (EMP).

Major elements, iron, magnesium, fluorine, chlorine, and sulphur were analysed with a CAMECA SX-50 wavelength-dispersive electron microprobe. Analytical conditions were 15 kV accelerating voltage and a beam current of 6 nA. A rastering electron beam (15 μm in diameter) was used for glass analyses in order to minimize Cl, S, and F migration, these being among the first elements measured during an analysis. Major elements were measured for 20 s, F and Cl for 30 s, and S for 300 s to raise the detection limit (145 ppm) for the analytical conditions used.

Trace-element analyses were performed with the SYXRF set-up at beamline L of HASYLAB (Hamburger Synchrotronstrahlungs-Labor) located at DESY (Deutsches Elektronen-Synchrotron) in Hamburg, Germany (Lechtenberg *et al.* 1996; Hansteen *et al.* 2000). Due to the limited interaction between the sample material and the X-ray photons, SYXRF is a completely non-destructive method for volatile analysis. A fundamental parameter approach was used to

compute element concentrations (Vincze *et al.* 1993; Hansteen *et al.* 2000). The sample-specific thickness, density, and Fe concentration, measured by electron microprobe, were used as input variables for the simulation procedure. Detection limits for an acquisition time of 3600 s were between 0.1 and 0.3 μg/g (Z=55; Br) and 7–10 μg/g (Z=64; Gd).

Compositional parameters of halogens and sulphur in the Laacher See magma

The Laacher See matrix glasses show a distinct compositional change throughout the entire tephra sequence, indicating that a chemically zoned magma reservoir was tapped during the eruption. Concentrations of MgO, FeO* (=all Fe recalculated as FeO), CaO, and Sr are highest in ULST matrix glasses (corresponding with the lower parts of the magma reservoir) and decrease towards LLST (upper parts of magma chamber). Concentrations of Nb, Zr, Th, Y, and rare-earth elements (REE) increase from ULST to LLST. Apparently, the concentrations represent a particular position in the magma reservoir. We can therefore relate matrix glasses (MG) and glass inclusions (GI) to specific positions in the magma chamber, using chemical variation diagrams. Concentrations of volatile elements in the glass inclusions correlate positively with high-field-strength (HFS) elements, and reflect the zonation of the magma chamber prior to MG melt formation. Examples are Mo v. Nb, Br v. Nb or Mo v. Br, having low concentrations in

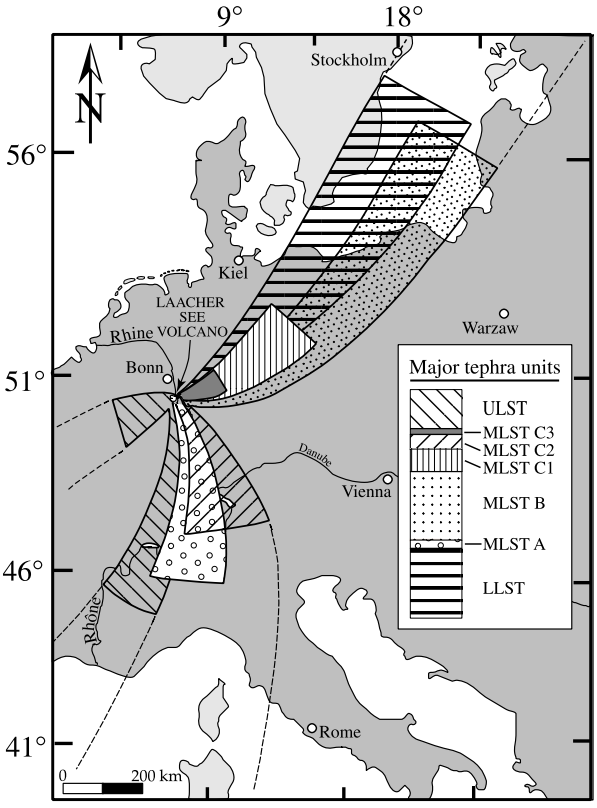

Fig. 1. Areal distribution of Laacher See tephra fallout (after van den Bogaard & Schmincke 1985). The volume of erupted melt has been estimated to be between 5.1 and 6.3 km^3 DRE (dense rock equivalent) (van den Bogaard & Schmincke 1985; Harms & Schmincke 2000). The proximal tephra sequence is subdivided into three major units: Lower Laacher See Tephra (LLST, first Plinian stage, dominantly fallout except for the most proximal facies), Middle Laacher See Tephra (MLST A, B, C; second Plinian stage, dominantly pyroclastic flows in the lower and alternating fallout and flow in the upper part) and Upper Laacher See Tephra (ULST, phreatomagmatic stage with dominantly surge breccias, dunes and flows).

deep parts of the magma chamber and high concentrations in the upper parts.

By comparing matrix glasses with glass inclusions, we can thus distinguish between those compositional patterns indicating late-magmatic volatile depletion and those representing late-magmatic enrichment. The covariation of the volatile elements Br and S (e.g. the representations of Br v. Nb or S v. MgO) indicate a depletion of both Br and S in MG chlorine concentrations (e.g. Cl v. MgO), and are significantly higher in GI as compared with MG fluorine correlations (e.g. F v. MgO), indicating a significant enrichment during formation of MG. Bromine provides the clearest evidence for the action of a fluid phase within the Laacher See magma chamber during formation of the MG melts. The matrix glasses are characterized by a plateau-like concentration of Br, which ranges between 3 and 7 μg/g, over the entire stratigraphic sequence. The plateau provides evidence that a simple mechanism, and therefore a single process, controlled the concentration levels. Most likely, this was the release of a fluid phase limited by the quenching rate of the melt during the eruption.

The ratios Cl/Br, F/Br and SO_2*/Br v. Br (SO_2*=all S recalculated as SO_2) increase strongly with decreasing Br concentration, i.e. with increasing depth within the magma chamber, as shown in Figures 2 and 3.

This indicates selective enrichment of S, F, and Cl relative to Br. Breakdown of mafic phenocrysts in the lower parts of the magma chamber must be taken into account as a source of fluorine and chlorine. This is supported by the roof-ward increase in the amphibole/clinopyroxene phenocryst ratio of the magma chamber (Tait *et al.* 1989). The ratios F/Br and Cl/Br of amphibole, phlogopite and biotite (occurring as phenocrysts and corroded crystals) are possible end-members of the related paths, and provide evidence for contamination by these phases. Amphibole, phlogopite/biotite and apatite appear to be incompatible for bromine (bromine concentrations <0.5 μg/g). This indicates that contamination through assimilation cannot provide enrichment of bromine over F and Cl, and will increase F/Br and Cl/Br ratios. The breakdown of hauyne has no significant influence (<2 vol. %), because the apparent partition coefficient of Br in hauyne and coexisting glass inclusions (concentration in hauyne/concentration in melt) is close to unity ($KBr^{Hau/liq} \approx 1$). This is also indicated by the plot of SO_2*/Br v. Br (Fig. 3).

The absence of pyrrhotite in the upper parts of the Laacher See magma chamber supports the

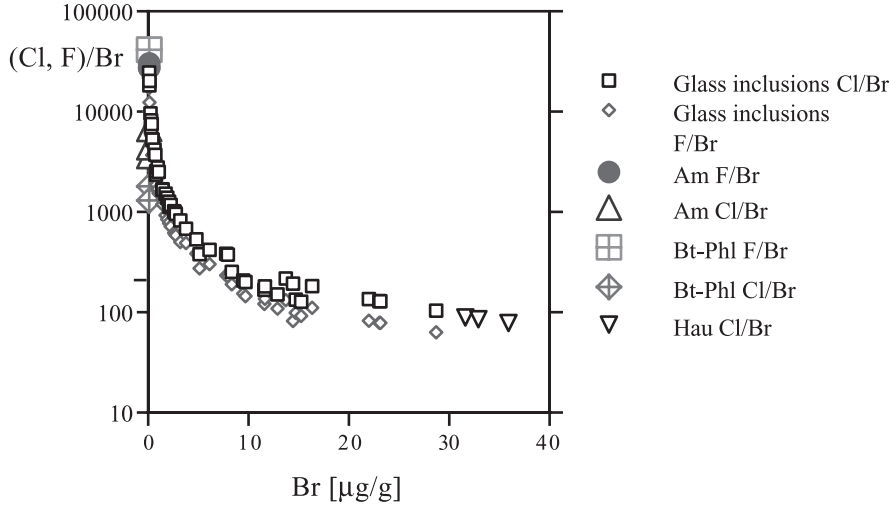

Fig. 2. Representation of F/Br and Cl/Br v. Br. Low Br concentrations in the glass inclusions are representative of the deep regions of the chamber, while high concentrations occur in the upper part. The relative enrichment of Cl and F at low Br concentrations appears to be related to the breakdown of amphibole and/or biotite and phlogopite, which define possible end-members at low bromine concentrations. Element ratios were estimated through a best fit by $F/Br=1586.162*Br^{-0.989}$ ($r^2=0.996$); and $Cl/Br=2379.676*Br^{-0.981}$ ($r^2=0.991$). The Cl/Br ratio of the average continental crust is from Bureau *et al*. (2000). The Cl/Br and F/Br ratios of amphibole and phlogopite/biotite represent a minimum value (Br was below the detection limit of about 0.1 μg/g). Am=amphibole, Bt–Phl=biotite/phylogopite, Hau=hauyne.

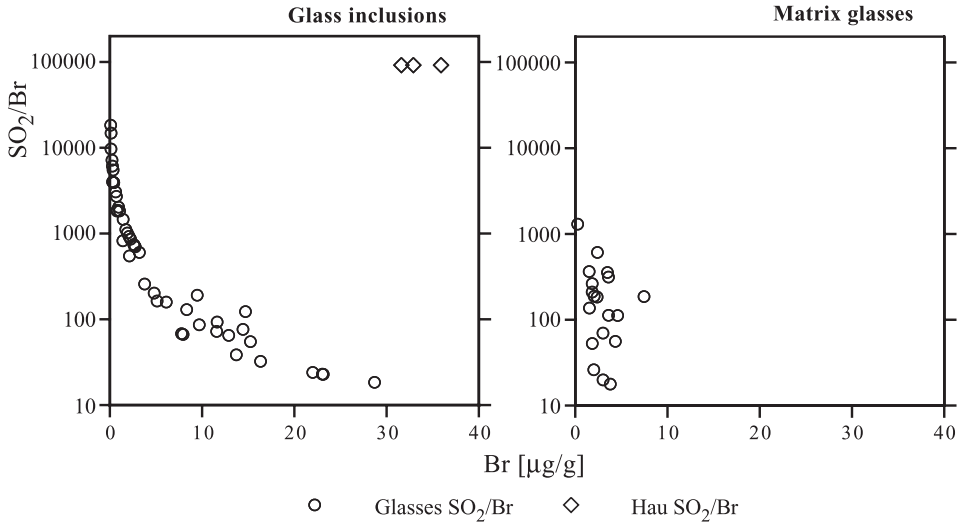

Fig. 3. Sulphur/bromine ratios v. bromine contents of glass inclusions and matrix glasses. Glass inclusions with low Br concentrations are representative of the deep regions of the chamber, and high concentrations of the upper part. The concentrations in matrix glasses show the plateau concentration of bromine over the entire tephra profile. The strong hyperbolic increase of the ratio SO_2*/Br for the glass inclusions, with decreasing Br concentrations, indicates that sulphur has been added to the Laacher See magma and cannot be explained by the breakdown of hauyne. The decrease of SO_2*/Br with decreasing Br concentrations during formation of the matrix glass melts is probably controlled by the release of a fluid phase. Element ratios were estimated through a best fit by $SO_2*/Br = 1467.334*Br^{-1.200}$ ($r^2 = 0.966$).

hypothesis of sulphur enrichment of the phonolite melt through sulphide breakdown. Pyrrhotite globules ($Fe_{1-x}S$, ≤10 μm in diameter) are trapped in mafic phonolite glass inclusions and in amphibole, clinopyroxene, plagioclase, and titanite crystals in the lowermost parts of the magma chamber (ULST to MLSTB). This demonstrates that the Laacher See melt was FeS-saturated in the deep chamber, and provides evidence that sulphide has been resorbed in shallower parts of the magma chamber, probably due to an increase in oxygen fugacity.

Estimate of the volatile release

Estimation of volatiles released during an eruption by subtraction of concentrations in matrix glasses from concentrations in the glass inclusions (the so-called 'petrological method') can lead to severe underestimation of the atmospheric input (see Scaillet & Pichavant, 2003, Chapter 3, this volume). For SO_2, data obtained with the petrological method can yield an apparent release one to two orders of magnitude less than those obtained by other methods such as satellite data (e.g. Andres *et al.* 1991). Due to late-stage volatile enrichment of the Laacher See MG melts, involving breakdown of amphibole (±phlogopite, biotite) and of sulphide-bearing phases (most likely FeS, $CuFeS_2$), the eruptive release of most of the volatiles cannot be estimated by the petrological method. Unrealistically low or even negative masses of volatiles (fluorine) released into the atmosphere would be obtained. We therefore determined the bromine release using a combination of the petrological method and known fluid/melt partition coefficients (Bureau *et al.* 2000).

We calculated the emissions from the Br release as follows. The definitions of the concentrations of the masses m_i of a component I (index: i) in the melt (index: liq) and in the fluid (index: f) with masses m_{liq} and m_f are:

$$C_i^{liq} = m_i/m_{liq} \text{ and } C_i^{f} = m_i/m_f \quad (1)$$

The partition coefficient of component i distributed between fluid and melt is:

$$D_i^{f/liq} = C_i^{f}/C_i^{liq} \quad (2)$$

The concentrations of components i and Br in the fluid are given by:

$$C_i^{f} = D_i^{f/liq} C_i^{liq} \text{ and } C_{Br}{}^{f} = D_{Br}{}^{f/liq} C_{Br}{}^{liq} \quad (3)$$

Combining equations 1 and 3 yields:

$$m_i^f = m_{Br}^f (D_i^{f/liq}/D_{Br}^{f/liq})(C_i^{liq}/C_{Br}^{liq}) \quad (4)$$

The masses m_i^f and m_{Br}^f are released from the melt into the fluid. In order to determine the atmospheric release of component i we assume that the fluid is completely released to the atmosphere, $m_i^{atm} \approx m_i^f$. The release of Br, m_{Br}^f, must be estimated independently. The apparent saturation concentration of a Br-bearing fluid is reflected in the MG plateau concentrations for Br of approximately 3–7 μg/g. We estimate the ratio C_i^{liq}/C_{Br}^{liq} from a representation of C_{Br}^{liq} through a best fit with a function of the type $C_i^{liq}/C_{Br}^{liq} = A(C_{Br}^{liq})^B$, where A and B are constants. The ratio C_i^{liq}/C_{Br}^{liq} reflects degassing at best through its minimum ratio, whereas higher values are progressively controlled through contamination.

One has to take into account that a considerable fraction of the fluid possibly consisted of H_2S. The partition coefficient for sulphur is strongly dependent on the oxygen fugacity fO_2, varying from $D_S^{f/liq}=47$ (high fO_2; fluid consists predominantly of SO_2) up to $D_S^{f/liq}=468\pm32$ (predominantly H_2S; Keppler 1999). A $D_{H_2O}^{f/liq}=100/6.55=15.27$ is taken as an approximation for the concentration of H_2O in glasses quenched from experimentally melted phonolite glass coexisting with aqueous fluid (Carroll & Blank 1997). As an extrapolation to multicomponent fluids, we use $D_{H_2O}^{f/liq}=95/6.55=14.5$. We determined the Br release to the atmosphere using the formula (GI: glass inclusions; MG: matrix glasses):

$$m_{Br} = (C_{Br}^{GI} - C_{Br}^{MG})\rho_{liq}\Phi_{liq}V_{liq} \quad (5)$$

through the difference $C_{Br}^{GI} - C_{Br}^{MG}$ between Br concentrations in glass inclusions of phenocrysts (clinopyroxene, hauyne, titanite, amphibole) and in MG, where $_{liq}$ is the density of the melt, and $\Phi_{liq}=0.97$ the mass fraction of melt relative to other phases. V_{liq} is the volume of magma from which the fluid component i was released. We assume that the melt density was 2300 kg/m^3 over the entire magma volume. The Br saturation concentration in melt was $C_{Br}^{MG}\approx3$–7 μg/g. Lower Br concentrations do not contribute to degassing. Only magma batches corresponding with LLST and MLST stratigraphic positions contribute to Br degassing (estimated volume $V_{liq}=4$ km^3 DRE). Deeper stratigraphic levels did not contribute to Br degassing, because the pre-eruptive concentration was below the MG concentration. The difference of volatile concentrations caused by fluid release is $C_{Br}^{GI} - C_{Br}^{MG}=17$–13 μg/g.

We determined therefore the mass M of released fluid components using the difference of bromine concentrations in glass inclusions and matrix glasses, with $M = M_{Br}(D/D_{Br})(C_m/C_{m,Br})$, whereby M=mass of released volatile, M_{Br}=bromine mass; $D = C_{fluid}/C_{melt}$: partition coefficients; and C_m=volatile concentration at maximum Br concentration. The resulting mass of released bromine is $M_{Br}=0.19$–0.29 Tg. Using equation 4, we obtain the following mass releases M in Tg: F=0.214, Cl=11.5, I=<0.03, S=3.38 (assuming pure SO_2) or S=52.4 (assuming pure H_2S), and H_2O=698. The resulting estimates for volatile release during the Laacher See eruption, and the parameters involved, are summarized in Table 1.

For comparison, the SO_2 emission can be crudely estimated from the relationship between the volcanic explosivity index VEI (Newhall & Self 1982) and typical SO_2 emissions for non-arc volcanoes (Schnetzler *et al.* 1997). The VEI for the Laacher See eruption is VEI=4–5 (column height 18 km, volume of erupted tephra 10^9–10^{10} m^3). This yields an average SO_2 release of about $mSO_2=10\pm5$ Tg. This suggests that at least part of the sulphur was released in the form of H_2S.

Processes in the eruption column

Radical chemistry in a volcanic plume

During the rise of volcanic emissions from the crater to the stratosphere, i.e. within the volcanic plume, radical chemistry is negligible. This has been shown by sensitivity studies with a chemistry box module under volcanic conditions. The rise time of volcanic gases from the crater to the stratosphere is of the order of 10 minutes. This is shorter than the characteristic time of chemical transformations under normal atmospheric conditions. In addition, the optical depth of the eruption column is so high (due to the presence of ash) that photochemistry is strongly suppressed. Thus, the volcanic gas injection into the stratosphere is controlled by the plume height and by scavenging through hydrometeors, which might remove the gases from the atmosphere when they precipitate.

Scavenging by liquid droplets

The physical solubility of an arbitrary gas, *HA*, in water is described by the Henry coefficient *He*. Within the context of this work, all concentrations are given in units of mol. kg^{-1} $_{tot.mass}$. In these units, *He* increases with increasing liquid water content:

$$He = \frac{[HA]_{aq}}{[HA]_g} \quad (6)$$

Table 1. *Estimation of volatile release and related parameters for the 12 900 year BP Laacher See eruption.*

Component	Plateau concentration in matrix glass (μg/g)	Concentration in melt C_i (μg/g)	Partition coefficient $D_i^{f/liq}$	Erupted mass m_i (Tg)
F	1617	231	0.18	0.214
Cl	1932	276	8.1	11.5
Br	7	1	17.5	0.19–0.29
I	<0.5	<0.07	104	<0.03
SO_2* (pure SO_2 or H_2S)	SO_2*=68 ± 17; Br=3.8	14	SO_2: 47–137 H_2S: 468	Pure SO_2: 3.38 Pure H_2S: 52.4
H_2O	65 500	9357	14.5	698

The partition coefficient is $D_i^{f/liq}=C_i^f/C_i^{liq}$. m_i is the mass in the fluid phase, which is assumed to be completely released to the atmosphere: $m_i^f=m_{Br}{}^f\,(D_i^{f/liq}/D_{Br}{}^{f/liq})(C_i^{liq}/C_{Br}{}^{liq})$.

where the parentheses indicate the species concentration in the gas and water phase, *g* and *aq*, respectively. *He* refers to the pure physical solubility equilibrium of a gas in water, regardless of its subsequent fate in the droplet. However, acidic gases undergo acid–base reactions like $HA \leftrightarrow A^- + H^+$, described by the dissociation constant K_s:

$$Ks = \frac{[A^-]_{aq}\,[H^+]_{aq}}{[HA]_{aq}} \tag{7}$$

The dissociation reaction in the liquid phase enhances the uptake of gases in droplets. The total solubility, given by the effective Henry coefficient *He**, is then also a function of the pH value:

$$He^* = \frac{[HA]_{aq} + [A^-]_{aq}}{[HA]_g} = He\left(1 + \frac{K_s}{[H^+]}\right) \tag{8}$$

Corresponding expressions are valid for two-protonic acids like H_2S and SO_2. All equilibrium constants are temperature dependent according to the van't Hoff equation:

$$K = K_0 \exp\left(\frac{\Delta H}{R}\left(\frac{1}{T} - \frac{1}{T_0}\right)\right) \tag{9}$$

The Henry coefficients generally increase as the temperature decreases, reflecting a greater solubility at lower temperatures. The reaction enthalpy, ΔH, is the energy change involved with dissolution of gases in water, and T_0=289 K is the reference temperature for the values of the Henry coefficients and the acidity constants, K_0, which are taken from Sander and Crutzen (1996). The solubility of HCl in water is about four orders of magnitude greater than that of the sulphur containing gases. Hence, HCl is likely to be completely scavenged by water drops, and its revolatilization would require a drastic decrease of the system's liquid water content. The timescales to adjust to phase equilibrium are of the order of a fraction of a second for the dissolution of slightly soluble gases; however, highly soluble gases need much longer times (e.g. Seinfeld & Pandis 1997). The time to establish phase equilibrium increases with droplet radius and liquid water content. The characteristic times needed to achieve the Henry's law equilibrium (including subsequent dissociation reaction inside the droplets) are long when compared with the model time step, of about 0.5 s simulation time in ATHAM, especially for HCl. Hence, we have to consider the time dependency of phase transfer.

We assume that the characteristic phase transfer time of gases into the liquid phase, and vice versa, is dominated by gas phase diffusion and interfacial mass transfer. For simplicity we suppose that the droplets are internally well mixed and that rapid dissociation equilibria in the aqueous phase are instantaneously reached. We neglect any other liquid phase reactions. A further simplification is achieved by applying the steady-state approximation: species concentrations, fluxes, and reaction rates are no longer a function of time during one model time step (Schwartz 1986). The phase transfer rate of volatiles into liquid droplets with subsequent dissociation reactions of acidic gases in the liquid phase is then proportional to the deviation from the solubility equilibrium:

$$\frac{\partial}{\partial t} c_{aq} = -\frac{1}{L}\frac{\partial}{\partial t} c_g = k_t (c_{g,\infty} - c_{g,eq}) \tag{10}$$

where $c_{aq}=[HA]_{aq}+[A^-]_{aq}$ is the total concentration in the aqueous phase and $c_{g,eq}=[HA]_g$ denotes the concentration in the gas phase at the droplet surface, given by He^* in equation 1. The $c_{g,\infty}$ is the gas concentration in the undisturbed environment, and L, in $kg_{aq}\ kg^{-1}_{tot.mass}$, the liquid water content. The phase transfer constant k_t, in s^{-1}, is defined as the inverse sum of the characteristic times of mass transport of a gas to the drop surface τ_{dg} and that across the air–water interface, including the possible establishment of solubility equilibrium locally at the interface τ_i (Schwartz 1986).

$$k_t=(\tau_{dg}+\tau_i)^{-1}=(\frac{r^2}{3D_g}+\frac{4r}{3\bar{\nu}\alpha})^{-1} \qquad (11)$$

where

$$D_g=2\lambda\bar{\nu}(1+0.22\mathrm{Re}^{0.5}) \qquad (12)$$

and

$$\bar{\nu}=\sqrt{\frac{8RT}{M\pi}} \qquad (13)$$

r is the volume mean radius of the particle, in m, D_g the gas phase diffusion coefficient in m^2/s, including the effects of turbulence caused by circulation around a falling drop, Re is the Reynolds number. $\bar{\nu}$ denotes the mean speed of gas molecules from the kinetic gas theory in m/s, R=8.3143 mol/kJ is the general gas constant, M, in kg/mol., is the molecular weight, and λ, in m, the mean free path in air. The sticking coefficients $\alpha(HCl)=0.2$ and $\alpha(SO_2)=0.11$ are taken from DeMore *et al.* (1997). The value for H_2S used, $\alpha(H_2S)=0.1$, was chosen to be in the range of the other values, because no observational data were available.

The resulting equations are linearized by using a Taylor expansion, with truncation after the first term, as in Newton's method (Press *et al.* 1992); the Jacobian is iteratively solved with an efficient realization of a Gauss elimination (M. Oberhuber, pers. comm. 1996). We use an implicit time stepping procedure to solve the set of stiff non-linear equations.

Scavenging by ice particles

Field studies and a number of laboratory experiments have indicated that ice crystals are able to scavenge gaseous species from the surrounding air (for references, see Diehl *et al.* 1998). The solubility of gases in ice is much lower than in liquid water, since ions are rejected by the ice matrix. The gas uptake is dependent on the type of gas, temperature, and crystalline structure of the ice. In addition, gas uptake is different for growing and non-growing ice (Pruppacher & Klett 1997). It has been observed that the contamination of ice does not correspond with the thermodynamic equilibrium solubility of chemical species in ice. Among others, Valdez & Dawson (1984), Mitra *et al.* (1992), Diehl *et al.* (1995), and Thibert & Dominé (1997) performed laboratory experiments to investigate the uptake of gases by ice crystals. The experiments indicated that the diffusivities of electrolytes in ice are very low compared with liquid water values. Species, once incorporated in ice, will not be able to considerably change their position within the crystal. Thus the phase equilibrium cannot be established after the initial gas incorporation within the time of a volcanic eruption simulated with ATHAM.

It has been observed that the contamination of ice does not correspond with the thermodynamic equilibrium solubility of chemical species in ice, but is ruled by condensation kinetics (e.g. Dominé *et al.* 1995; Diehl *et al.* 1995). Gaseous species are incorporated during diffusional ice particle growth, due to the deposition of water vapour. Gas scavenging is proportional to the mass of water vapour converted to ice. This process is parameterized in ATHAM, according to the ideas of Dominé *et al.* (1995), and Dominé and Thibert (1996):

$$x_i=\frac{n_c\alpha_c}{n_{H_2O}\alpha_{H_2O}}\frac{\bar{\nu}_c}{\bar{\nu}_{H_2O}} \qquad (14)$$

where α denotes the sticking coefficient and $\bar{\nu}$ the mean speed of gas molecules from the kinetic gas theory given in equation 13. The low diffusion constant of electrolytes in ice prevents volcanic volatiles, once incorporated into ice crystals, from re-evaporating. Using the expressions for the mean gas speed $\bar{\nu}$ given in equation 13 we obtain for the time-dependent change of a chemical species due to incorporation into ice crystals:

$$\frac{\partial}{\partial t}c_i=-\frac{\partial}{\partial t}c_g=\frac{\partial}{\partial t}q_i\frac{c_g}{q_v}\frac{\alpha_c}{\alpha_{H_2O}}\sqrt{\frac{M_{H_2O}}{M_c}} \qquad (15)$$

where c_i and c_g are the contents of chemicals in ice and in the gas phase in mol $kg^{-1}_{tot.mass}$, respectively. q_i and q_v denote the specific contents

of ice and water vapour in kg $kg^{-1}_{tot.mass}$. The sticking coefficient $\alpha(HCl)=0.3$ is taken from DeMore *et al.* (1997). For SO_2 and H_2S we assume the same values as for liquid water, $\alpha(SO_2)=0.11$ and $\alpha(H_2S)=0.1$, because no observational data were available. We apply for water vapour $\alpha(HO_2)=1$. In the context of this work, we neglect the temperature dependence of α. Considering the limited data available, the sticking coefficients applied in our simulations may hold for a first investigation of the significance of gas incorporation into ice particles. The efficiency factor $f_{inc,c}$

$$f_{inc,c} = \frac{\alpha_c}{\alpha_{H_2O}} \sqrt{\frac{M_{H_2O}}{M_c}} \tag{16}$$

is for HCl $f_{inc,HCl}=0.21$, for SO_2 $f_{inc,}SO_2=0.06$ and for H_2S $f_{inc,}H_2S=0.07$, respectively. Hence, HCl will be most effectively incorporated into ice particles.

Release of gases from ice

Diehl *et al.* (1995) observed in laboratory experiments during the sublimation of polluted ice, that pure water vapour is transferred to the gas phase at first, leading to increased concentrations of dissolved species in the remaining hydrometeor. After reaching a critical contamination, simultaneous sublimation of water vapour and dissolved chemicals occurs. However, no quantitative information of this process is available. Probably, the release of solutes depends on the rate of water vapour transfer. There might be no time to build up an accumulation zone during fast sublimation, and instead, solutes and water vapour leave the ice crystal simultaneously. In this study, we assume that the fraction of chemicals released to the gas phase is proportional to that of sublimating water vapour. For consistency, the amount of released gases is weighted by the inverse of the factor applied in the gas incorporation equation (equation 15). The behaviour of the species concentration caused by release of gases from ice particles is given by:

$$\frac{\partial}{\partial t} c_g = -\frac{\partial}{\partial t} c_i = \frac{\partial}{\partial t} q_v \frac{c_i}{q_i} \frac{\alpha_{H_2O}}{\alpha_c} \sqrt{\frac{M_c}{M_{H_2O}}} \tag{17}$$

Transfer of solutes during microphysical processes

Coagulation of different hydrometeor classes leads to a mixture of the original solutions, thus producing new droplets or ice particles with average species concentrations. The retention coefficients for gases in water during freezing of the solution seem to be dependent on the species' nature. Iribarne & Pyshnov (1990) demonstrated experimentally that, during freezing of liquid droplets, some highly soluble chemical species, among them HCl, are totally retained in the ice phase. Iribarne (1990) found that S(IV) dissolved in droplets is partially evolved as SO_2 during freezing; the retention of S(IV) increases with increasing growth rate of the ice particles. In a volcanic eruption column, liquid droplets experience a strong temperature decrease because of the quick ascent (about 100 m/s) leading to rapid freezing. Here, we assume that the total amount of the chemicals contained in the liquid phase is shifted into the ice phase during droplet freezing. Correspondingly, the species previously contained in the ice phase are completely transferred into the liquid phase during ice melting. The time-dependent change of the specific content c_x, in mol $kg^{-1}_{tot.mass}$, of a chemical species contained in a hydrometeor q_x, in kg $kg^{-1}_{tot.mass}$, is assumed to be proportional to that of the hydrometeor. It is calculated from the sum over the microphysical processes involved with the particular type of hydrometeor, x, under consideration:

$$\frac{\partial}{\partial t} c_x = \sum_{procs} \frac{c_x}{q_x} \left(\frac{\partial}{\partial t} q_x\right). \tag{18}$$

Condensation of water vapour on liquid hydrometeors leads to dilution of the solutions; evaporation of water drops causes an increase of the concentration. At the same time, the phase transfer kinetics of chemical species work towards a phase equilibrium. Total evaporation releases the species back into the gas phase, neglecting a possible aerosol formation due to the crystallisation of salt particles. The treatment of incorporation and resublimation of chemicals into ice particles during their growth has been shown above. The processes included in the scavenging module guarantee that volcanic species, initially erupted at the vent as gases, can be contained in each class of hydrometeors. Once scavenged, they experience all microphysical processes, as shown in Figure 4.

Numerical simulations with the plume model ATHAM

The ATHAM model is described in detail by Oberhuber *et al.* (1998) and Herzog (1998). This model is capable of dealing with the development of the dynamics in space and time, and it

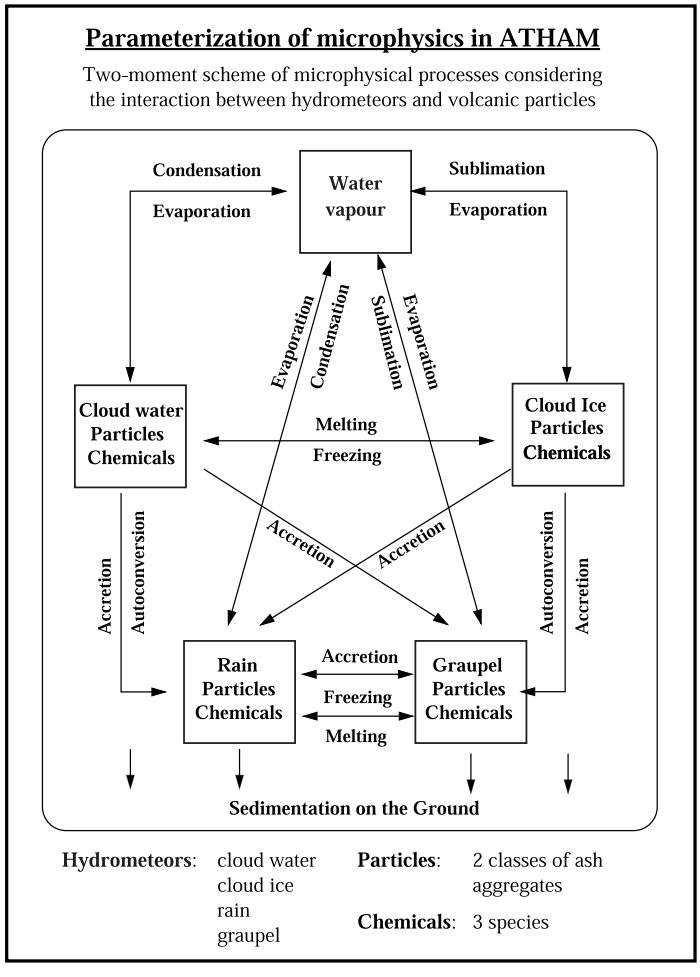

Fig. 4. Scheme of the processes included in the scavenging module.

considers the microphysics and physicochemical processes taking place in volcanic clouds (Textor 1999; Textor *et al.* 2003*a, b*). It has been tested for different applications (Graf *et al.* 1999, Trentmann *et al.* 2001). Here, we use the ATHAM model to simulate the development of a Plinian eruption cloud in the atmosphere, focusing on the fate of sulphur and halogen species.

In the ATHAM model, the full set of Navier–Stokes equations is solved using a finite difference method with an implicit time step scheme on a regular grid. For a complete description of the model equations, see Herzog (1998) and Oberhuber *et al.* (1998). In this study we use five modules:

- The dynamic part solves the Navier–Stokes equation for the gas–particle mixture, and includes the transport of active tracers (Herzog 1998; Oberhuber *et al.* 1998).
- The turbulence closure scheme delivers the turbulent exchange coefficients for each dynamic quantity, thereby describing the entrainment of ambient air into the plume (Herzog 1998, Oberhuber *et al.* 1998).
- The cloud microphysics describes condensation of water vapour and formation of precipitation. All phases of water are included: vapour, liquid, and solid. The feedback of thermal energy changes on the dynamics is considered (Herzog *et al.* 1998; Graf *et al.* 1999; Textor 1999, 2003*a*).
- The ash module describes particle growth and aggregation based on microphysical interactions between hydrometeors and ash (Textor 1999; Textor *et al.* 2003*a*).

- The scavenging module calculates dissolution of volcanic gases into droplets, including the dissociating reactions of the acidic gases, and the incorporation of volatiles into ice particles. The redistribution of species contained in hydrometeors due to microphysical processes is considered (Textor 1999; Textor *et al.* 2003*b*).

The numerical experiments using the ATHAM model refer to processes close to the volcano. We focus on the exploration of the fate of volcanic gases within the eruption column, which is relevant for the mesoscale effects of the eruption on time-scales of several hours. We are interested in the amount of material injected into the stratosphere, and not in the distribution of volcanic emissions on the global scale.

Numerical experiment of an explosive volcanic eruption similar to the Laacher See eruption, 12 900 years BP

For this study we used the axi-symmetrical version of the plume model formulated in cylindrical coordinates, as it is more economical in terms of computer memory and time. Cross-wind cannot be considered in this scheme, but the dilution of the mixture by entrainment of surrounding air is captured well (Herzog 1998). The simulations are performed on a stretched lattice with 126×126 grid points. The model domain was 200 km in the horizontal and 50 km in the vertical direction. In the centre of the model domain we use a spatial resolution of 120 m, coarsening to about 5 km at the margins. This grid choice permits the simulation of the full plume development with restricted computer resources without disturbances from the model boundaries for a simulation time of 90 min. The numerical experiments begin just after the earliest mixing of the erupting gas–particle mixture with the atmosphere, after equilibration with atmospheric pressure. The volcanic forcing in the model refers to the situation just after the decompression phase; small-scale processes in the vicinity of the crater in the high-temperature regime are not resolved within the concept of ATHAM. We focus on processes occurring in the plume in the spatial scales of about 100 m to some tens of km. The input of volcanic material during the eruption is specified by defining the vertical velocity, the temperature, and the composition of the ejecta at five vent grid points.

The volcanic and environmental conditions are based on the phonolitic Plinian eruption of the Laacher See volcano. The chemical species are initialized in concentrations according to the conditions of the eruption, as given in the previous section.

- Geometry of the volcano: height 400 m, crater diameter 600 m, the crater depth 200 m.
- Vent exit velocity 350m/s, vent temperature 1000 K.
- Mean volume radii of the two ash classes: 2.5 and 50 μm, with the larger class contributing 60 % of the total ash mass.
- Particle density $\delta = 1800$ kg/m^3.
- Gas mass fraction of the gas–particle-mixture: 6 wt%, where water vapour contributes a fraction of 85 %.
- Gases

total	6	wt%
H_2O	4.35	wt%
SO_2	0.154	wt%
HCl	8.42×10^{-2}	wt%
HBr	2.59×10^{-3}	wt%

- Density of the gas–particle mixture: 3.9 kg/m^3
- Ash mass eruption rate $\approx 4\times10^8$ kg/s.

For initializing the environmental profiles of temperature and humidity, we used typical data for mid-latitude summer (McClatchey *et al.* 1972). The tropopause is at 13 km, as shown in Figure 5.

The simulation time was 90 min, and the eruption lasted for 30 min. Within the first 10 s, the eruption velocity was increased to its maximum, followed by a phase of 27 min of continuous eruption. During the last 3 min of the eruption, the vent exit velocity was reduced to zero again. We continued the simulation for additional 60 min in order to investigate the post-eruptive development of the volcanic plume.

The dynamic and environmental conditions of the volcanic eruption are constant for all experiments. The dispersal of volcanic material in the atmosphere, especially the injection into the stratosphere, depends on the volcanic conditions (composition of the magma, strength of the eruption) and on the meteorological conditions (stability of the atmosphere, lateral wind) in the ambient atmosphere. The impact of the environmental conditions on the plume's shape and height has been investigated by Herzog (1998) and Graf *et al.* (1999) through numerical simulations with ATHAM, and is not the subject of this study.

Results

Volcanic particles

The plume that develops under the conditions employed in this study reaches the stratosphere; the neutral buoyancy height is at 15 km. The time

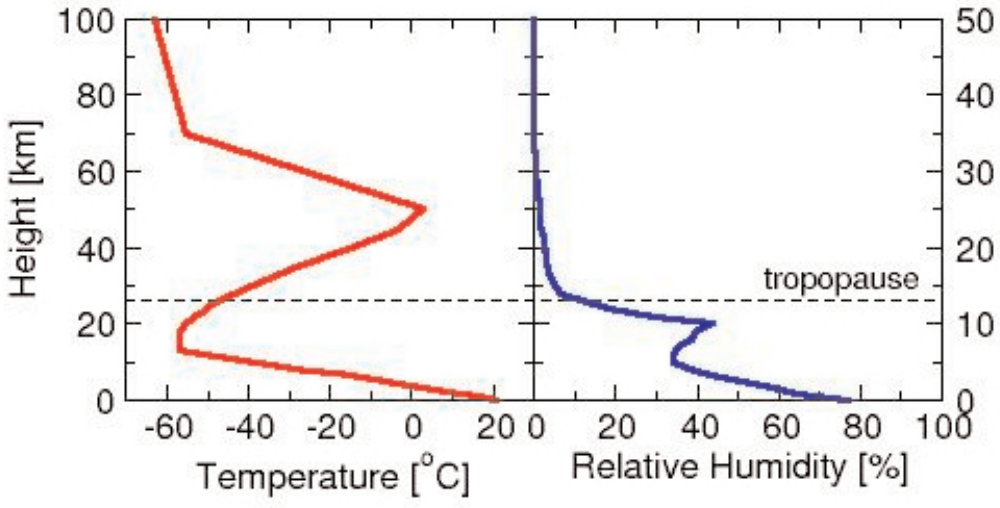

Fig. 5. Atmospheric background profiles for temperature and relative humidity.

to rise from the crater to the tropopause at ~13 km is about 5 min; vertical velocities in the central rising zone are higher than 40 m/s on average. Smaller ash particles (radius 2.5 μm), cloud ice and volcanic gases form a layer in the stratosphere at the neutral buoyancy height, which spreads horizontally. Sedimentation removes larger particles from the stratosphere. ~10% by mass (in the following, all percentages refer to % by mass) of the particles are deposited 60 min after the eruption ends, indicating that gas particle separation is quite efficient in our simulation. The plume of volcanic particles after 30 min of eruption, and the post-eruptive ash clouds at 60 and 90 min after the end of the eruption are shown in Figure 6 a–c. The ash dispersal and the effect of aggregation on the plume height and shape are discussed elsewhere (Textor *et al.* 2003*a*).

Hydrometeors

Figure 7 a–b shows the plume of hydrometeors, and the vertical profiles at 30 min, and 60 min after the end of the eruption. The hydrometeors in our simulation contain volcanic ash (which is shown in Fig. 6), as determined by parameterisation of the microphysics in ATHAM (Textor *et al.* 2003*a*). Hence, water or ice is part of hydrometeor–ash-aggregates. As a result of the dry conditions of the surrounding atmosphere, the hydrometeor fraction in these aggregates is less than 20% at all grid points.

Condensation mainly occurs in the rising zone; the condensation level is at about 5 km height. Liquid water exists only in the central lower eruption column, and frozen hydrometeors predominate (>99% of the total hydrometeor mass). Most of the ice can be found in the umbrella region. A layer of cloud ice forms in the stratosphere, graupel (larger ice particles) slowly precipitates into the troposphere. At 90 min simulation time, i.e. 60 min after the end of the eruption, only ice exists in the plume. Before melting to rain, graupel evaporates, and precipitation cannot be detected at the ground.

Volcanic gases

The plume of total HCl at 30 min, and 60 min after the end of the eruption, is shown in Figure 8 a–b. Note that a large fraction of HCl reaches the stratosphere and, like the particles and hydrometeors, it spreads horizontally at the neutral buoyancy height. Some of this HCl, however, is scavenged by particles and transported back into the troposphere, as can be seen in Figure 8b.

The behaviour of volcanic gases in the eruption column is determined by the scavenging efficiency. The concentration of volcanic gases in different phases is dependent on the solubility of the individual species. The hydrogen halides HCl and HBr are highly soluble in liquid water, whereas the sulphur species SO_2 and H_2S are only slightly soluble. The vertical profiles of the

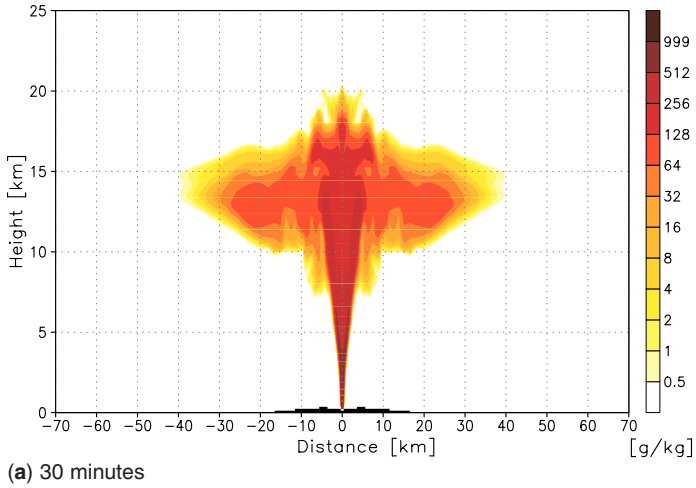

(**a**) 30 minutes

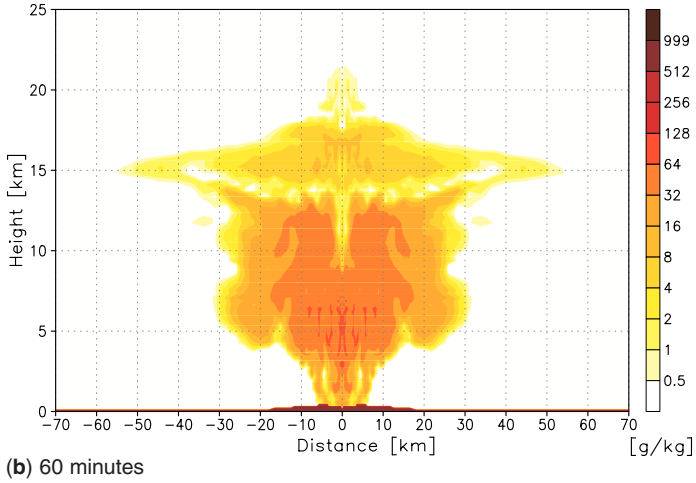

(**b**) 60 minutes

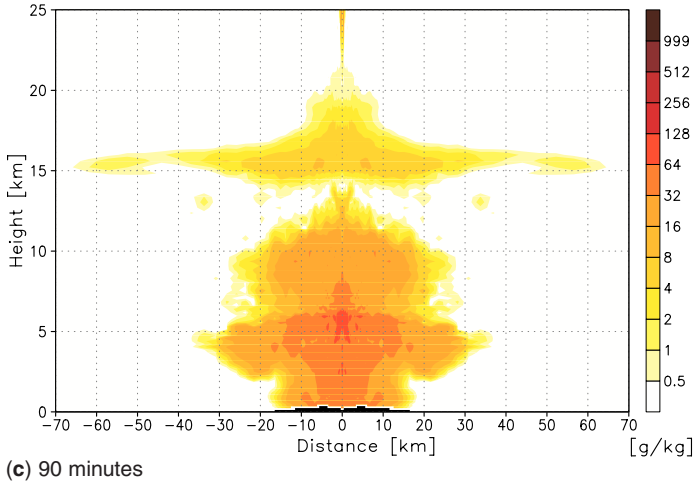

(**c**) 90 minutes

Fig. 6. The plume of volcanic particles at (**a**) 30 min after the start of the eruption; and the post-eruptive ash clouds at (**b**) 60 and (**c**) 90 min of simulation. Ash mass mixing ratio is in g/kg total mass.

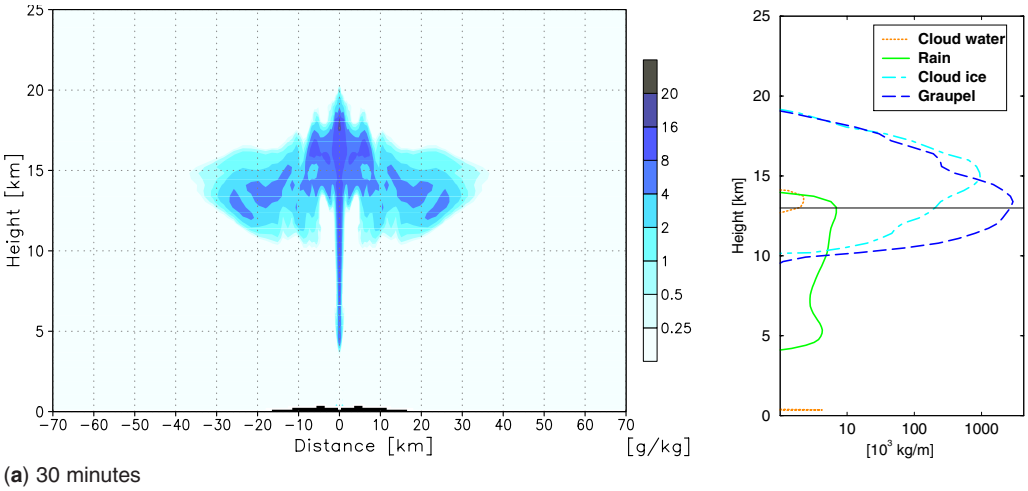

(**a**) 30 minutes

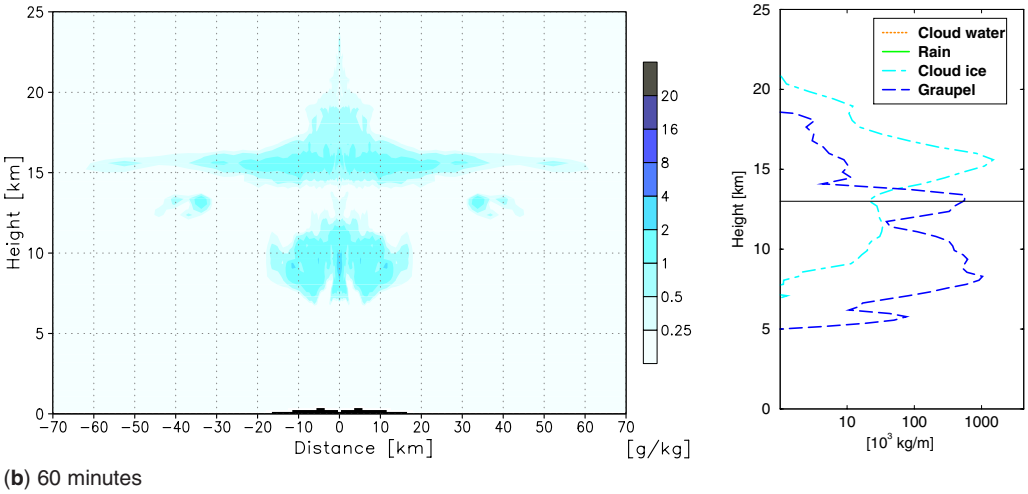

(**b**) 60 minutes

Fig. 7. Plume of hydrometeors (sum over all categories) and vertical profiles (individual categories integrated at each height level at (**a**) 30 min and (**b**) 90 min of the simulation.

species contained in all hydrometeor categories and in the gas phases are shown in Figure 9.

The halogens are contained in all phases of hydrometeors. These gases are scavenged by liquid water drops in the central rising zone of the plume. However, only ~1% by mass of the erupted amount is contained in liquid water, more then 70% by mass of the erupted halogens remain in the gas phase, because very little water is available. Droplet freezing and direct gas incorporation transfers halogens into cloud ice and graupel.

The sulphur gases, SO_2 and H_2S, are also contained in all phases of hydrometeors but about 95% of the erupted gases remain in the gas phase. Scavenging is mainly caused by direct gas incorporation. Due to their lower solubility, the scavenging by liquid water is insignificant (~0.005%).

Figure 10 shows the fractions of HCl and SO_2 erupted that reach the stratosphere. The species are shown in all phases. For comparison, the fraction of an inert gas in the stratosphere is included. This gas is not scavenged by hydrometeors, i.e. its stratospheric injection of ~85% is determined only by the plume height. More than 60% of the erupted halogens reach the stratosphere, and the scavenging efficiency is 30% when compared with the potential injection of the inert gas. Approximately 25% of the halogens in the stratosphere is contained in cloud ice. The growth of ice to graupel, and subsequent precipitation, would remove halogen species from the stratosphere.

More than 80% of the total erupted sulphur reaches the stratosphere. The scavenging effici-

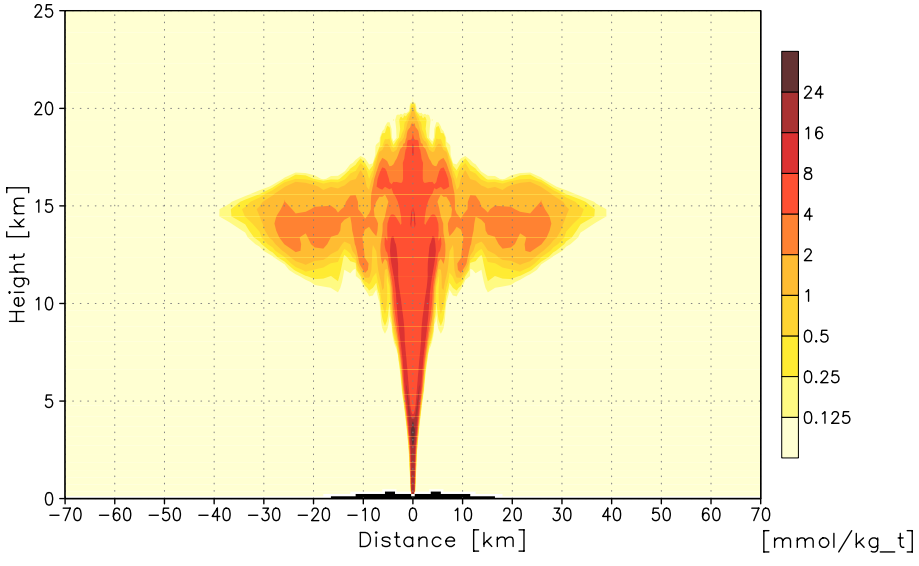

Fig. 8. The HCl eruption: plumes of total HCl (sum over HCl in all phases) (**a**) 30 min into the eruption, and (**b**) 60 min after the end of the eruption (90 min simulation time) in mmol/kg.

ency is 5% when compared with the potential injection of an inert gas; ~2% of the sulphur in the stratosphere is contained in ice.

Conclusions

We investigated zoned phonolitic Plinian eruption of Laacher See volcano, (12 900 years BP). The ratios Cl/Br, F/Br, and SO_2*/Br v. Br increase strongly with decreasing Br concentration, i.e. with increasing depth of the magma chamber. Breakdown of mafic phenocrysts in the lower parts of the magma chamber must be taken into account as a source of fluorine and chlorine. Amphibole, phlogopite/biotite, and apatite appear to be incompatible for bromine

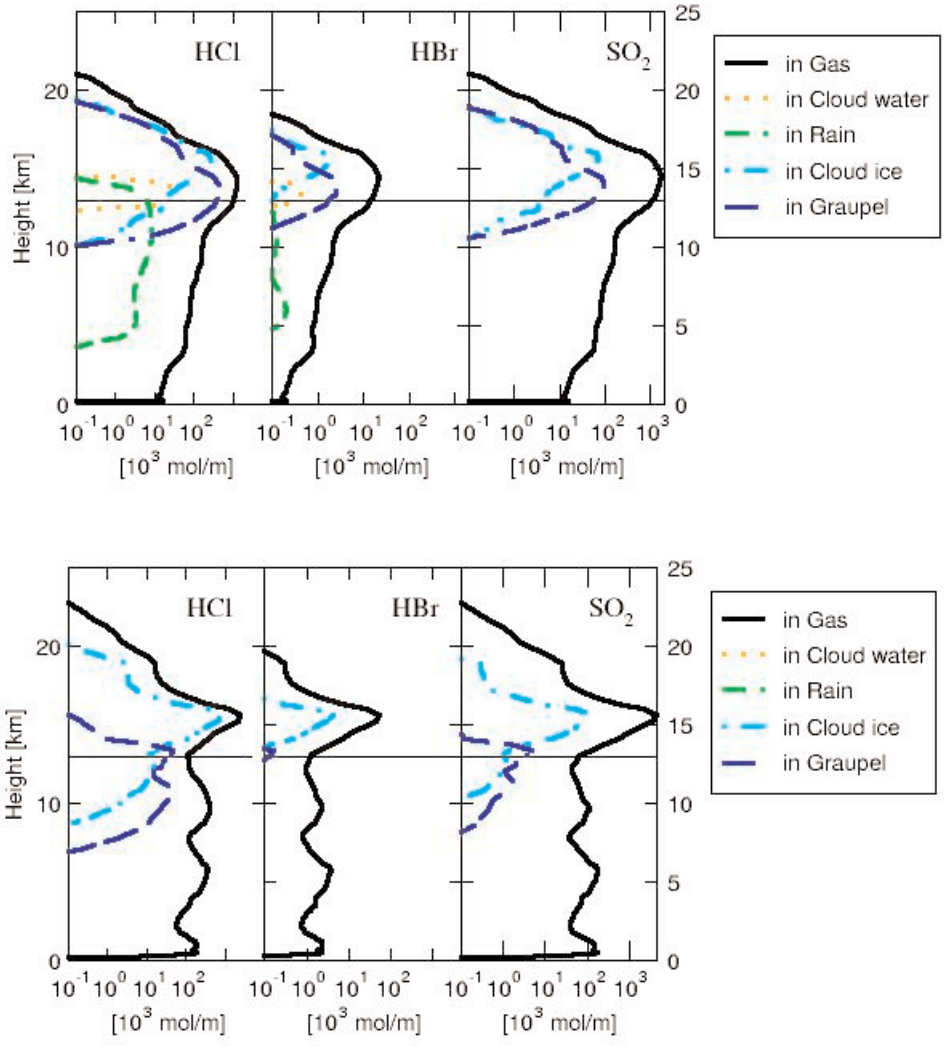

Fig. 9. Vertical profiles of HCl, HBr, and SO_2 in different phases, in mol/m, at (**a**) 30 and (**b**) 90 min of simulation.

(bromine concentrations <0.5 μg/g). In addition, the Laacher See melt was FeS-saturated in deep parts of the magma chamber, and provides evidence that sulphide has been resorbed in the shallower parts of the magma chamber, probably due to the increase of oxygen fugacity, fO_2. We therefore determined the masses of released fluid components, using the difference of bromine concentrations in glass inclusions and matrix glasses, and recalculating to volatile concentration at maximum Br concentration. The resulting masses M in Tg are: F=0.21, Cl=11.5, Br=0.19 −0.29, I:<0.03, S=3.38 (assuming pure SO_2) or S=52.4 (assuming pure H_2S), and H_2O=698.

We performed a numerical experiment with the plume model ATHAM for the conditions of the Laacher See eruption. The focus of this study was the investigation of the fate of volcanic gases in the plume and their injection into the stratosphere. The eruption column penetrated the tropopause, the neutral buoyancy height being reached about 2 km above it. The simulations showed that all volcanic gas species reach the neutral buoyancy height in the stratosphere. Without scavenging, about 85% of the gases erupted at the vent would reach the stratosphere. However, volcanic gases are partly scavenged by hydrometeors. The scavenging efficiency depends

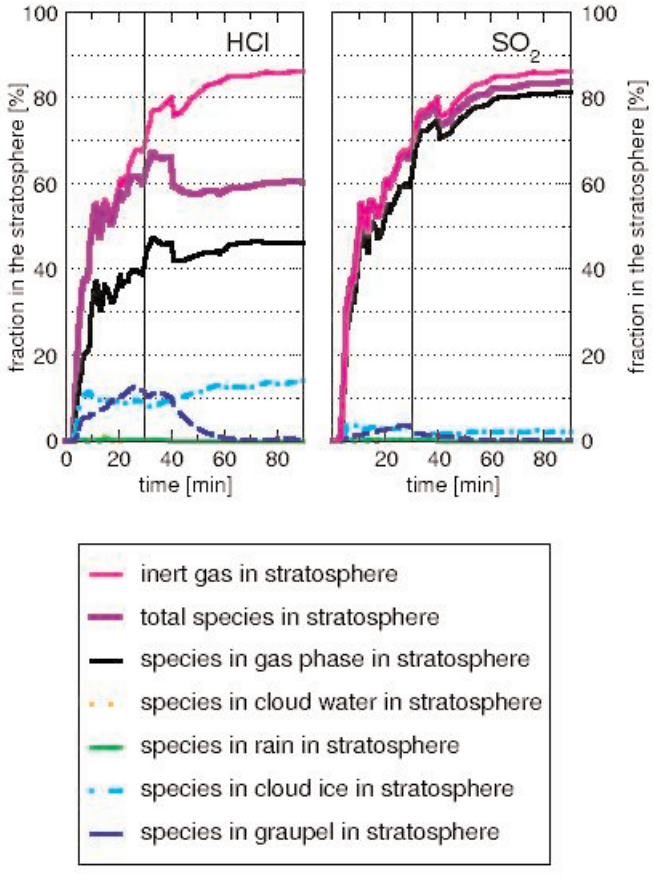

Fig. 10. Fraction of total erupted HCl (left plot) and SO_2 (right plot) that reached the stratosphere.

on the individual water solubility of the species, and on the incorporation in ice during diffusional growth. For the dry troposphere through which the Laacher See plume rose, we found a scavenging efficiency of only 30% for hydrogen halides, despite their high water solubility, and of 5% for the sulphur species.

The majority of the hydrometeors were frozen to ice, due to the fast plume rise and the great height of the eruption column. Hence, only a small amount of HCl and HBr was scavenged by liquid water in the rising plume. A small fraction of volcanic gases was incorporated into ice particles, but many of these were transported upwards and reached the neutral buoyancy height as well.

A large amount of SO_2 and H_2S stays in the gas phase at high levels in the umbrella region. The sulphur species are only slightly soluble in liquid water, and so they are not removed by cloud and raindrops at lower heights. However, they might be scavenged by frozen hydrometeors via direct gas incorporation during diffusional growth of ice. The proposed mechanism of gas trapping in ice within a volcanic plume is supported by observations of eruption clouds in which a lot of water was present in the plume due to interaction with sea-water: extremely high amounts of ice were accompanied by unusually low SO_2 concentrations. However, the exact value of the scavenging efficiency for the individual species is sensitive to the sticking probabilities of gas molecules at the ice particle's surface. These are based on limited data, which should be improved.

The scavenging efficiency depends on the availability of hydrometeors, and on the fraction of liquid water in the plume. The Laacher See eruption occurred in a dry environment. In a wet troposphere, the entrainment of humid ambient

air increases the hydrometeor content. This might strongly enhance the scavenging of volcanic gases. A co-ignimbrite plume with a slower vertical velocity might also contain a much higher content of liquid water, which could efficiently remove HCl from the atmosphere.

The ATHAM simulations showed that the highest fraction of volcanic species that reached the umbrella region was still in the gas phase. Earlier numerical studies by Tabazadeh and Turco (1993) indicated that HCl was totally removed from the plume by scavenging in supercooled drops, while SO_2 was almost completely injected into the stratosphere. However, these authors did not consider freezing of hydrometeors, and probably overestimated the amount of liquid water in the plume. In addition, they did not consider scavenging by ice particles. Our numerical experiments show that, in a dry atmosphere, the amount of water condensing in a plume might not be sufficient to completely scavenge HCl, such that a large proportion can reach the stratosphere.

Volcanic species once scavenged by hydrometeors are not necessarily transferred to the troposphere and deposited at the ground via precipitation of contaminated rain. The ATHAM simulations show that precipitation evaporated in the dry atmosphere before reaching the ground, thus releasing the gases back to the troposphere. A large fraction of contaminated hydrometeors even reach the stratosphere. Gravitational settling would remove species from the stratosphere, and sublimation would release them in the gas phase. Our simulations suggest that the secondary increase of SO_2 during the first days after a stratospheric injection, which has been observed in some satellite data of eruption clouds, could be caused by SO_2 release from ice particles. The efficiency of gas scavenging by ice through co-condensation with water vapour depends on the growth mechanism of ice in the eruption column, and on the sticking coefficient of SO_2 on the ice particle. Further laboratory and field work are necessary to clarify this process.

The final amount of volcanic gases in the stratosphere depends on the fate of contaminated ice particles in the stratosphere. The effect of explosive volcanic eruptions on stratospheric chemistry and microphysics, and on the global climate, is determined by the specific volcanic and atmospheric conditions during and after the eruption.

Reviews by anonymous referees are greatly appreciated. This research was supported by the Volkswagen Foundation under the project EVA (emission of volcanic volatiles into the atmosphere).

References

Andres, R.J., Rose, W. I., Kyle, P. R., deSilva, S., Francis, P., Gardeweg, M. & Roa, H. M. 1991. Excessive sulfur dioxide emissions from Chilean volcanoes. *Journal of Volcanology and Geothermal Research*, **46**, 323–329.

Angell, J. K. 1997. Estimated impact of Agung, El Chichón and Pinatubo volcanic eruptions on global and regional total ozone after adjustment for the QBO. *Geophysical Research Letters*, **24(6)**, 647–650.

Berndt, J., Holtz, F. & Koepke, J. 2001. Experimental constraints on storage conditions in the chemically zoned phonolitic magma chamber of the Laacher See volcano. *Contributions to Mineralogy and Petrology*, **140**, 469–486.

Bluth, G. J. S, Doiron, S. D., Schnetzler, C. C, Krueger, A. J., Walter, L. S. 1992. Global tracking of the SO_2 clouds from the June, 1991 Mount Pinatubo eruptions. *Geophysical Research Letters*, **19**, 151–154.

Bluth, G. J. S., Scott, C. J., Sprod, I. E., Schnetzler, C. C., Krueger, A. J. & Walter, L. S. 1995. Explosive SO_2 emissions from the 1992 eruptions of Mount Spurr, Alaska. *US Geological Survey Bulletin,* **2139**, 37–45.

Brasseur, G. P., Granier, C. & Walters, S. 1990. Future changes in stratospheric ozone and the role of heterogeneous chemistry. *Nature*, **348,** 626–628.

Bureau, H., Keppler, H. & Métrich, N. 2000. Volcanic degassing of bromine and iodine: experimental fluid/melt partitioning data and applications to stratospheric chemistry. *Earth and Planetary Science Letters*, **183**, 51–60.

Carroll, M. R. & Blank, J. G. 1997. The solubility of H_2O in phonolitic melts. *American Mineralogist*, **82**, 549–556.

Charlson, R. J., Langner, J., Rodhe, H., Leovy, C. B. & Warren, S. G. 1991. Perturbation of the Northern Hemisphere radiative balance by backscattering from anthropogenic sulfate aerosols. *Tellus*, **43A–B(4)**, 152–163

Charlson, R. J., Schwartz, S. E., Hales, J. M., Cess, R. D., Coakley Jr, J. A., Hansen, J. E. & Hoffman, D. J. 1992. Climate forcing by anthropogenic aerosols. *Science*, **255**, 423–430.

Daniel, J. S., Solomon, S. & Albritton, D. L. 1995. On the evaluation of halocarbon radiative forcing and global warming potentials, *Journal of Geophysical Research*, **100**, 1271–1285.

DeMore, W. B., Sander, S. P., *et al.* 1997. *Chemical Kinetics and Photochemical Data for Use in Stratospheric Modeling.* Evaluation No. **12**; Jet Propulsion Laboratory: Pasadena, CA.

Diehl, K., Mitra, S. K. & Pruppacher, H. R. 1995. A laboratory study of the uptake of HNO_3 and HCl vapor by snow crystals and ice spheres at temperatures between 0-degrees-C and –40-degrees-C. *Atmospheric Environment*, **29(9)**, 975–981

Diehl, K., Mitra, S. K. & Pruppacher, H. R. 1998. A laboratory study on the uptake of HCl, HNO_3 and SO_2 gas by ice crystals and the effect of these gases on the evaporation rate of the crystals. *Atmospheric Research*, **48**, 235–244.

Dominé, F. & Thibert, E. 1996. Mechanism of incorporation of trace gases in ice grown from the gas phase. *Geophysical Research Letters*, **23(24)**, 3627–3630.

Dominé, F., Thibert, E. & Silvente, E. 1995. Determining past atmospheric HCl mixing ratios from ice core analyses. *Journal of Atmospheric Chemistry*, **21(2)**, 165–186.

Gerlach, T. M. & Casadevall, T. J. 1986. Fumarole emissions at Mount St. Helens Volcano, June 1980 to October 1981: degassing of a magma–hydrothermal system. *Journal of Volcanology and Geothermal Research*, **28**, 141–160.

Glaze, L. S., Baloga, S. M., Wilson, L. 1997. Transport of atmospheric water vapor by volcanic eruption columns. *Journal of Geophysical Research*, **102(D5)**, 6099–6108.

Gleason, J. F. *et al.* 1993. Record low global ozone in 1992. *Science*, **260**, 523–526.

Graf, H.-F., Herzog, M, Oberhuber, J. M. & Textor, C. 1999. The effect of environmental conditions on volcanic plume rise. *Journal of Geophysical Research*, **104**, 24 309–24 320.

Granier, C. & Brasseur, G. 1992. Impact of heterogeneous chemistry on model predictions of ozone changes. *Journal of Geophysical Research*, **97**, 18 015–18 033.

Hansteen, T. H., Sachs, P. M., Lechtenberg, F. 2000. Synchrotron–XRF microprobe analysis of silicate reference standards using fundamental-parameter quantification. *European Journal of Mineralogy*, **12**, 25–31.

Harms, E. 1998. Volatile composition and syn-eruptive degassing of the Laacher See phonolite magma (12,900 yr BP). *Reihe Geowissenschaften*, **39**.

Harms, E., Schmincke, H.-U. 2000. Volatile composition of the phonolitic Laacher See magma (12900 yr BP): implications for syn-eruptive degassing of S, F, Cl, and H_2O. *Contributions to Mineralogy and Petrology*, **138**, 84–98.

Herzog, M. 1998. *Simulation der Dynamik eines Multikomponentensystems am Beispiel vulkanischer Eruptionswolken*. PhD Thesis, University of Hamburg.

Herzog, M., Graf, H.-F., Textor, C. & Oberhuber, J. M. 1998. The effect of phase changes of water on the development of volcanic plumes. *Journal of Volcanology and Geothermal Research*, **87**, 55–74.

Hofmann, D. J. & Solomon, S. 1989. Ozone destruction through heterogeneous chemistry following the eruption of El Chichon. *Journal of Geophysical Research*, **94**, 5029–5041.

Iribarne, J. V. & Pyshnov, T. 1990. The effect of freezing on the compositions of supercooled droplets – I. retention of HCl, NH_3 and H_2O_2. *Atmospheric Environment,* **24A(2)**, 383–387.

Iribarne, J. V., Pyshnov, T. & Naik, B. 1990. The effect of freezing on the compositions of supercooled droplets – II. Retention of S(IV). *Atmospheric Environment*, **24A(2)**, 389–398.

Keppler, H. 1999. Experimental evidence for the source of excess sulphur in explosive volcanic eruptions. *Science*, **284**, 1652–1654.

Krotkov, N. A. & Krueger, A. J. 2000. Composition of the plume from the February 26, 2000 eruption of Mt. Hekla, Iceland: a combined satellite – model study. *EOS, Transactions of the American Geophysical Union*, **81(48)**, Fall Meeting Supplement, Abstract V61B–10.

Lechtenberg, F., Garbe, S., *et al.* 1996. The x-ray fluorescence measurement place at beamline L of Hasylab, J. *Trace and Microprobe Techniques*, **14(3)**, 561–587.

McKeen, S. A., Liu, S. C. & Kiang, C. S. 1984. On the chemistry of stratospheric SO_2 from volcanic eruptions. *Journal of Geophysical Research*, **89(D3)**, 4873–4881.

McClatchey, R. A., Fenn, R. W., Selby, J. E. A., Volz, F. E. & Garing, J. S. 1972. *Optical Properties of the Atmosphere*, 3rd edn, Environmental Research Papers, No. 411.

Mankin, W. G. & Coffey, M. T. 1984. Increased stratospheric hydrogen chloride in the El Chichon cloud. *Science*, **226(4671)**, 170–172.

Mankin, W. G., Coffey, M. T. & Goldman, A. 1992. Airborne observations of SO_2, HCl, and O_3 in the stratospheric plume of the Pinatubo volcano in July 1991. *Geophysical Research Letters*, **19**, 179–182.

Mayberry, G. C., Rose, W. I. & Bluth, G. J. S. 2001. Dynamics of the volcanic and meteorological clouds produced by the December 26, 1997 eruption of Soufrière Hills volcano, Montserrat, W.I. *In:* Druitt, T. & Kokelaar, P. (eds) *The Eruption of Soufrière Hills Volcano, Montserrat, 1995–99*, Geological Society of London, Memoir, **21**, 539–555

Mitra, S. K., Waltrop, A., Flossmann, A., Pruppacher, H. R. 1992. A windtunnel and theoretical investigation to test various theories for the absorption of SO_2 by drops of pure water and water drops containing H_2O_2 and $(NH_4)_2SO_4$. *In:* Schwartz, S. E. & Slinn, W. G. N. (eds) *Precipitation Scavenging and Atmospheric–Surface Exchange*, Vol. I of The Georgii Volume: Precipitation Scavenging Processes, Hemispheric Publishing Corporation, Washington DC 123–141.

Montzka, S. A., Butler, J. H., *et al.* 1996. Decline in the tropospheric abundance of halogen from halocarbons: Implications for stratospheric ozone depletion. *Science*, **272(5266)**, 1318–1322.

Newhall, C. G. & Self, S. 1982. The volcanic explosivity index (VEI): an estimate of explosivity magnitude for historic volcanism. *Journal of Geophysical Research*, **87**, 1231–1238.

Oberhuber, J. M., Herzog, M., Graf, H.-F., Schwanke K 1998. Volcanic plume simulation on large scales. *Journal of Volcanology and Geothermal Research*, **87**, 29–53.

Press, W. H., Teukolsky, S. A., Vetterling, W. T., Flannery, B.P. 1992. *Numerical Recipes in FORTRAN, the Art of Scientific Computing*, Cambridge University Press, 2nd edition.

Pruppacher, H. R. & Klett, J. D. 1997. *Microphysics of Cloud and Precipitation*, Kluwer Academic Publishers, The Hague, 2nd edition.

Rose, W. I., Delene, D. J., Schneider, D. J., Bluth, G. J. S., Krueger, A. J., Sprod, I., McKee, C., Davies, H., Ernst, G. G. J. 1995. Ice in the 1994

Rabaul Eruption Cloud: implications for volcano hazard and atmospheric effects. *Nature*, **375**, 477–479.

Rose, W. I., Bluth, G. J. S. & Ernst, G. G. J. 2000. Integrating retrievals of volcanic cloud characteristics from satellite remote sensors: a summary. *Philosophical Transactions of the Royal Society of London Series A – Mathematical, Physical and Engineering Sciences*, **358(1770)**, 1585–1606.

Rose, W. I., Bluth, G. J. S., Riley, C. M., Watson, I. M, Yu, T. & Ernst, G. G. J. 2000. Potential mitigation of volcanic cloud hazards using satellite data – a case study of the February 2000 Hekla Event and an unexpected NASA DC8 encounter. *EOS – Transactions of the American Geophysical Union*, **81(48)**, Fall Meeting Supplement, Abstract V61B-09.

Rose, W. I., Bluth, G. J. S., Schneider, D. J., Ernst, G. G. J., Riley, C. M. & McGimsey, R. G. 2001. Observations of 1992 Crater Peak/Spurr volcanic clouds in their first few days of atmospheric residence. *Journal of Geology*, **109**, 677–694.

Sachs, P. M. & Harms, E. 1998. The injection of bromine into the atmosphere by the Plinian Laacher See eruption (Germany), 12000 BP: relevance for the global stratospheric ozone layer. *EOS – Transactions of the American Geophysical Union*, **79**, 936 (abstract).

Sachs, P. M. & Harms, E. 2000. Atmospheric release of Br, I, Cl, F and SO_2 by the Laacher See volcanic eruption (Germany), 12900 BP. *Berichte der Deutschen Mineralogischen Gesellschaft, Beiheft zum European Journal of Mineralogy*, **12**, 174.

Sander, R. & Crutzen, P. J. 1996. Model study indicating halogen activation and ozone destruction in polluted air masses transported to the sea. *Journal of Geophysical Research*, **101D**, 9121–9138.

Scaillet, B. & Pichavant, M. 2003. Experimental constraints on volatile abundances in arc magmas and their implications for degassing processes. *In*: Oppenheimer, C., Pyle, D. M. & Barclay, J. *Volcanic Degassing.* Geological Society, London, Special Publications, **213**, 23–52.

Schmincke, H. U., Park, C. & Harms, E. 1999. Evolution and environmental impacts of the eruption of Laacher See Volcano (Germany) 12,900 a BP. *Quaternary International*, **61**, 61–72.

Schneider, D. J. & Rose, W. I. 1994. Observations of the 1989–90 Redoubt Volcano eruption clouds using AVHRR Satellite Imagery. *In:* T. Casadevall (ed.) Proceedings of International Symposium on Volcanic Ash and Aviation Safety. *US Geological Survey Bulletin* **2047**, 405–418.

Schnetzler, C. C., Bluth, G. J. S., Krueger, A J. & Walter, L. S. 1997. A proposed volcanic sulphur dioxide index (VSI). *Journal of Geophysical Research*, **102(B9)**, 20 087–20 091.

Schwartz, S. E. 1986. Mass-transport considerations pertinent to aqueous phase reactions of gases in liquid-water clouds. *In: Chemistry of the Multiphase Atmosphere*. Jaeschke, W. (ed.), Springer-Verlag, Berlin.

Seinfeld, J. H. & Pandis, S. N. 1997. *Atmospheric Chemistry and Physics: from Air Pollution to Global Change*, John Wiley, New York.

Simkin, T. 1993. Terrestrial volcanism in space and time. *Annual Review of Earth and Planetary Sciences*, **21**, 427–452.

Solomon, S., Portmann, R W., Garcia, R. R., Thomason, L.W., Poole, L. R. & McCormick, M. P. 1996. The role of aerosol variations in anthropogenic ozone depletion at northern midlatitudes. *Journal of Geophysical Research*, **101**, 6713–6727.

Solomon, S., Portmann, R.W.,*et al.*. 1998. Ozone depletion at mid-latitudes: coupling of volcanic aerosols and temperature variability to anthropogenic chlorine. *Geophysical Research Letters*, **25(11)**, 1871–1874.

Stenchikov, G. L., Kirchner, I., *et al*. 1998. Radiative forcing from the 1991 Mount Pinatubo volcanic eruption. *Journal of Geophysical Research*, **103**, 13 837–13 857

Tabazadeh, A & Turco, R. P. 1993. Stratospheric chlorine injection by volcanic eruptions: HCl scavenging and implications for ozone. *Science*, **260**, 1082–1086.

Tait, S. R. 1988. Samples from the crystallising boundary layer of a zoned magma chamber. *Contributions to Mineralogy and Petrology*, **100**, 470–483.

Tait, S. R., Wörner, G. v. d., Bogaard, P., Schmincke, H.-U. 1989. Cumulate nodules as evidence for convective fractionation in a phonolite magma chamber. *Journal of Volcanology and Geothermal Research,* **37**, 21–37.

Textor, C 1999. *Numerical simulation of scavenging processes in explosive volcanic eruption clouds.* Dissertation, Max-Planck-Institut für Meteorologie, Examensarbeit 65, Hamburg.

Textor, C., Graf, H.-F., Herzog, M., Oberhuber, J. M., Rose, W. I. & Ernst, G. G. J. (2003*a*) Volcanic particles in explosive eruption columns, Part I and II: to be submitted to *Journal of Volcanology*.

Textor C., Graf H.-F., Herzog, M. & Oberhuber, J. M. (2003*b*) Injection of Gases into the Stratosphere by Explosive Volcanic Eruptions, *Journal Geophysical Research* (in press).

Thibert, E. & Dominé, F. 1997. Thermodynamics and kinetics of the solid solution of HCl in ice. *Journal of Physical Chemistry*, **101**, 3554–3565.

Trentmann, J., Andreae, M. O., Graf, H.-F., Hobbs, P. V., Ottmar, R. D. & Trautmann, T. 2001. Simulation of a biomass burning plume: comparison of model results with observations, *Journal of Geophysical Research.*

Tie, X. X. & Brasseur, G. 1995. The response of stratospheric ozone to volcanic eruptions – sensitivity to atmospheric chlorine loading. *Journal of Geophysical Research*, **22(22)**, 3035.

Valdez, M. P. & Dawson, G. A. 1984. Sulfur dioxide incorporation into ice depositing from the vapour. *Journal of Geophysical Research*, **23**, 39–68.

van den Bogaard, P., Schmincke, H.-U. 1985. Laacher See tephra: a widespread isochronous late Quternary tephra layer in central and northern Europe. *Geological Society of America Bulletin*, **96**, 1554–1571.

Varekamp, J. C., Luhr, J. F. & Prestegaard, K. I. 1984. The 1982 eruptions of El Chichón volcano

(Chiapas, Mexico): character of the eruptions, ash-fall deposits, and gas phase. *Journal of Volcanology and Geothermal Research*, **23**, 39–68.

Vincze, L., Janssens, K. & Adams, F. 1993. A general Monte Carlo simulation of energy dispersive X-ray fluorescence spectra. *Spectrochimica Acta*, **48B**, 553.

Wallace, L. & Livingston, W. 1992. The effect of the Pinatubo cloud on hydrogen chloride and hydrogen fluoride. *Geophysical Research Letters*, **19(12)**, 1209.

Westrich, H. R. & Gerlach, T. M. 1992. Magmatic gas source for the stratospheric SO_2 cloud from the June 15, 1991 eruption of Mount Pinatubo. *Geology*, **20**, 867–870.

Wilson, L. 1976. Explosive volcanic eruptions – III. Plinian eruption columns. *Geophysical Journal of the Royal Astronomical Society*, **45**, 543–556.

Woods, A. W. 1988. The fluid dynamics and thermodynamics of eruption columns. *Bulletin of Volcanology*, **50**, 169–193.

Woods, A W. 1993. Moist convection and the injection of volcanic ash into the atmosphere. Journal of Geophysical Research, **98**, 17 627–17 636.

Woods, D. C., Chuan, R. L. & Rose, W. I. 1985. Halite particles injected into the stratosphere by the 1982 El Chichón eruption. *Science*, **230**, 170–172

Wörner, G , Schmincke, H. U. 1984*a* Mineralogical and chemical zonation of the Laacher See sequence (East Eifel, Germany). *Journal of Petrology*, **25**, 805–835.

Wörner, G., Staudigel, H. & Zindler, A. 1985. Isotopic contraints on open system evolution of the Laacher See magma chamber (Eifel, West Germany). *Earth and Planetary Science Letters*, **75**, 37–49.

Wörner, G. & Schmincke, H. U. 1984*b*. Petrogenesis of the zoned Laacher See tephra sequence. *Journal of Petrology*, **25**, 836–851.